INSTITUTE OF PHYSICS PUBLISHING SEMICONDUCTOR SCIENCE AND TECHNOLOGY

Semicond. Sci. Technol. **19** (2004) 8–16 PII: S0268-1242(04)60273-2

Comparison of dark current, responsivity and detectivity in different intersubband infrared photodetectors

V Ryzhii[1], I Khmyrova[1], M Ryzhii[1] and V Mitin[2]

[1] Computer Solid State Physics Laboratory, University of Aizu, Aizu-Wakamatsu 965-8580, Japan

[2] Department of Electrical and Computer Engineering, Wayne State University, Detroit 48202, USA

E-mail: v-ryzhii@u-aizu.ac.jp

Received 28 February 2003, in final form 19 August 2003
Published 30 September 2003
Online at stacks.iop.org/SST/19/8 (DOI: 10.1088/0268-1242/19/1/002)

Abstract

This paper deals with the comparison of quantum well, quantum wire and quantum dot infrared photodetectors (QWIPs, QRIPs and QDIPs, respectively) based on physical analysis of the factors determining their operation. The operation of the devices under consideration is associated with the intersubband (intraband) electron transitions from the bound states in QWs, QRs and QDs into the continuum states owing to the absorption of infrared radiation. The redistribution of the electric potential across the device active region caused by the photoionization of QWs, QRs and QDs affects the electron injection from the emitting contact. The injection current provides the effect of current gain. Since the electron thermoemission and capture substantially determine the electric potential distribution and, therefore, the injection current, these processes are also crucial for the device performance. To compare the dark current, responsivity and detectivity of QWIPs, QRIPs and QDIPs we use simplified but rather general semi-phenomenological formulae which relate these device characteristics to the rates of the thermoemission and photoemission of electrons from and their capture to the QWs and the QR and QD arrays. These rates are expressed via the photoemission cross-section, capture probability and so on, and the structural parameters. Calculating the ratios of the QWIP, QRIP and QDIP characteristics using our semi-phenomenological model, we show that: the responsivity of QRIPs and QDIPs can be much higher than the responsivity of QWIPs, however, higher responsivity is inevitably accompanied by higher dark current; the detectivity of QRIPs and QDIPs with low-density arrays of relatively large QRs and QDs is lower than that of QWIPs; the detectivity of QRIPs and QDIPs based on dense arrays can significantly exceed the detectivity of QWIPs.

1. Introduction

Intersubband infrared photodetectors are conventionally made of single or multiple quantum well structures. Infrared technology on the basis of quantum well infrared photodetectors (QWIPs) utilizing the intersubband transitions from QWs has matured rapidly in the last several years ([1], see also references therein).

However, due to dipole selection rules, the intersubband transitions in the conduction band stimulated by infrared photons polarized in the QW plane is forbidden. This necessitates the use of different radiation coupling structures in QWIPs, for instance, gratings. The problem of infrared radiation (IR) coupling can be eliminated if electrons in the intersubband photodetector active region are confined in one or both lateral directions, in addition to the usual vertical

 © 2004 IOP Publishing Ltd Printed in the UK

confinement. Such a confinement can be realized in quantum dot [2] and quantum wire [3] infrared photodetectors (QDIPs and QRIPs, respectively) in which arrays of QDs and QRs are incorporated instead of QWs. As pointed out previously [2, 3], QDIPs and QRIPs, aside from the sensitivity to normal incident IR, can exhibit some other features which can be beneficial; for example, an elevated current gain caused by a reduced capture probability due to the phonon bottleneck effect and formation of repulsive potential barriers by charged QDs, a reduced rate of thermal emission of electrons from QDs and QRs because of an increased activation energy, etc. By now fabrication and experimental studies of InAs/GaAs, InGaAs/GaAs, InGaAs/InGaP and Ge/Si QDIPs were reported by several research groups [4–20]. The majority of QDIPs studied are based on QD structures with vertical electron (hole) transport (perpendicular to the QD arrays). Apart from such QDIPs, there are successful realizations of lateral QDIPs in which electrons propagate parallel to the QD arrays [20, 21]. Lateral electron confinement is also used in quantum grid infrared photodetectors (QGIPs) [22] and the so-called quantum dot-in-a-well infrared detectors (QDWIPs) [23]. The principles of QDIP operation, results of experimental studies of QDIPs and analysis of their features were reviewed in some recent publications [24–27]. However, the assessment of the QDIP (and QRIP) potential is still controversial, so we feel that a comparative analysis of different intersubband infrared photodetectors, namely QWIPs, QRIPs and QDIPs, is needed. In this paper, we compare QWIPs, QRIPs and QDIPs utilizing the analysis based on a semi-quantitative treatment (in line with [27]) of fundamental physical factors determining and limiting the operation of QWIPs, QDIPs and QRIPs.

2. Device structures and principles of operation

Most of QWIPs, QRIPs and QDIPs are based on vertical heterostructures consisting of one or several QWs or two-dimensional arrays of QRs or QDs separated by the barrier layers. The QW, QR or QD structures serving as the photodetector active region, where IR radiation is absorbed, are sandwiched between heavily doped emitter and collector contact layers. The active region can be either doped (with dopants of the same type as the contact layers) or undoped. Usually the photodetectors in question are made of n^+-N-n-N-n^+- or N^+-N-n-N-N^+-heterostructures with n^+- or N^+-contact layers, respectively, N-type barrier layers, and n-type QWs, QRs or QDs. Schematic view of vertical QWIP, QRIP and QDIP device structures is shown in figure 1. The absorption of IR is associated with the electron intersubband transitions from bound states in QWs, QRs or QDs into continuum states above the barriers or into excited quasi-bound states near the barrier top. The bound-to-continuum transitions or bound-to-quasi-bound transitions followed by fast escape into the continuum result in the photoionization of QWs, QRs or QDs and the appearance of mobile electrons. Bound electrons accumulated in QWs, QRs or QDs can create a significant space charge in the active region. In photodetectors made of N^+-N-n-N-N^+-heterostructures with the same material of the contact and barrier layers, the electrons are injected from the emitter to the active region overcoming a potential barrier in the latter formed solely by the space charge. Hence, the

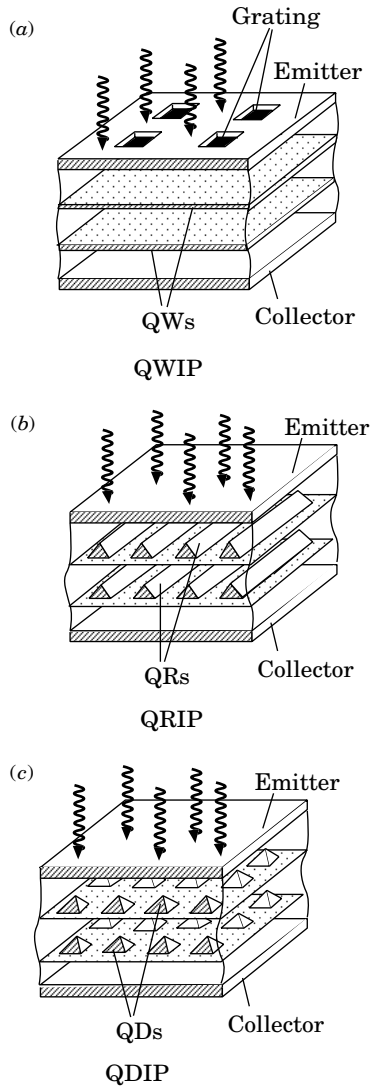

Figure 1. Schematic view of (*a*) QWIP, (*b*) QRIP and (*c*) QDIP device structures.

electron injection in such photodetectors is of thermionic origin. Due to a conduction band offset at the n^+-N heterointerface in n^+-N-n-N-n^+-photodetectors, the pertinent heterobarrier prevents the penetration of electrons from the emitter contact to the active region. However, a sufficiently strong electric field at this heterointerface, arisen due to the effect of the external electric field and the space charge, can result in a marked electron tunnelling to the active region providing the electron tunnelling injection. The QWIPs fabricated, studied and used in applications are primarily based on heterostructures with tunnelling injection, for example, on heterostructures with n^+-GaAs contact layers and QWs separated by N-AlGaAs barrier layers. In contrast, the majority of QDIPs is made of QD structures with the same material (e.g., GaAs) of the contact and barrier layers, although QDIPs with more exotic structures were investigated.

Under a bias voltage applied between the emitter and collector contacts the current across the active region depends on the applied voltage and the injection conditions (which are dictated by properties of the emitter contact). In normal

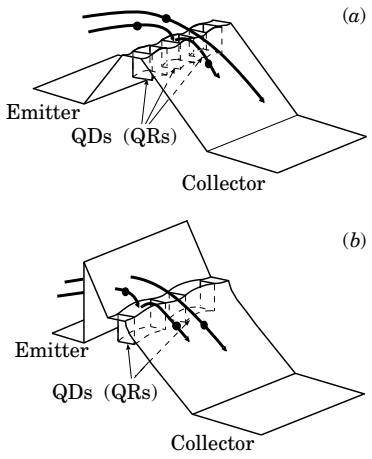

Figure 2. Schematic view of the conduction band profiles in single QR array QRIP or single QD array QDIP with thermionic (*a*) and tunnelling (*b*) injection. Arrows indicate electron trajectories in the active regions.

operation mode the current is limited by the space charge formed by electrons captured in QWs, or QRs or QDs. Under dark conditions, the space charge in the active region is determined by the balance between the processes of the electron capture into QWs (QRs or QDs) and the processes of the electron thermoemission (or tunnelling) from them. The space charge modifies the electric field distribution and affects the barrier at the emitter edge of the active region (in photodetectors with tunnelling injection) or leads to the formation of a controlled potential barrier inside this region (in photodetectors with thermionic injection). Under IR illumination, the photoionization of QWs, QRs or QDs shifts the balance between the electron capture and emission resulting in the redistribution of the electric field in the active region which, in turn, gives rise to a change in the injected current. The total current across the photodetectors includes two components: the current caused by the electrons emitted from QWs, QRs or QDs and the injected current. Since the capture of mobile electrons is usually rather slow process, the main portion of the dark current and photocurrent is due to the injection. The conduction band profiles in a QRIP and QDIP (with a single array of QRs and QDs, respectively) and the electron trajectories in their active regions are shown schematically in figure 2.

Thus, QWIPs, QRIPs and QDIPs operation is associated with the current across the photodetector active region limited by the bound space charge which is controlled by the incident IR radiation. Despite similarities in the QWIP, QRIP and QDIP principles of operation, there are some distinctions [2, 27]:

- Different degrees of the discreteness of the energy spectrum of bound electrons and, therefore, different statistics of these electrons, capture probability, and selection rules for intersubband transitions.
- Different spatial distributions of the electric potential in the active region, particularly in the lateral direction (virtually uniform in QWIPs and strongly nonuniform in QRIPs and QDIPs with low-density QR and QD arrays).
- Different dependences of the electron capture probability on the concentration (number) of bound electrons.

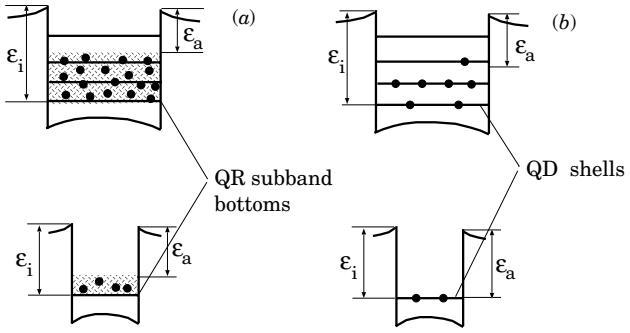

Figure 3. Energy spectra of (*a*) QRs and (*b*) QDs.

The above-mentioned distinctions can result in a marked quantitative variation of the device performance from one detector type to another, different approaches to the photodetector optimization, and different areas of applications. The characteristics of QRIP and QDIP can markedly depend on the lateral sizes of QRs and QDs. In QRIPs and QDIPs with QRs and QDs relatively large in the lateral direction (directions), each QR and QD can have many levels of the lateral quantization. In contrast, if the lateral size of QRs and both lateral sizes of QDs are small, the energy spectrum of such QRs can comprise only a single one-dimensional energy subband, whereas the energy spectrum of each QD consists of one discrete quantum level (shell). In the following, QRIPs with wide QRs and QDIPs with large QDs will be referred to as L-QRIPs and L-QDIPs, respectively. Analogously, QRIPs with narrow QRs and QDIPs with small QDs we will denote as S-QRIPs and S-QDIPs.

3. Thermoemission rate and dark current

The dark current and photocurrent in the photodetectors in question are determined, first of all, by the rates of thermionic emission from QWs (QR or QD arrays) and their photoemission by IR. In QWIPs with multiple QWs as well as in multi-array QDIPs and QRIPs, the contribution of different QWs or arrays can be slightly different. However, for a qualitative consideration, one can disregard this difference.

The interaction between the electron gas in each QW and the gas of mobile electrons propagating over continuum states above the inter-QW barriers is rather weak. Due to this, the energy distributions of electrons in QWs are given by the Fermi distribution function with the temperature coinciding with the lattice temperature T. At the same time, the electron sheet concentrations in QWs can be far from those when the whole electron system (which includes electrons in QWs, mobile electrons, and electrons in the contacts) is in equilibrium. In this case, the rate of thermoemission from QWs and QR (or QD) array is determined by the activation energy $\varepsilon_a = \varepsilon_i - \varepsilon_F$. Here ε_i and ε_F are the ionization energy of the QWs (QRs or QDs) and the Fermi energy in them, respectively (see figure 3).

The electron gas in QWs can be considered as a two-dimensional one, so the Fermi energy of electrons in QWs with respect to the bottom of the lowest subband equals

$$\varepsilon_F^{(\mathrm{QW})} = k_B T \ln\left[\exp\left(\frac{\pi\hbar^2\langle\Sigma\rangle}{mk_BT}\right) - 1\right] \simeq \frac{\pi\hbar^2\langle\Sigma\rangle}{m}, \qquad (1)$$

where $\langle\Sigma\rangle$ is average electron sheet concentration in QWs (or, in the following, in QR or QD arrays), $\hbar$ and k_B are the reduced Planck constant and the Boltzmann constant, respectively, and m is the electron mass. The last term in the right-hand side of equation (1) corresponds to $k_BT < \pi\hbar^2\langle\Sigma\rangle/m$.

Each relatively wide QR can have many one-dimensional subbands associated with the quantization of the energy of the electron lateral motion. Such QRs can be considered as strip-like QWs. Disregarding quasi-discreteness of the electron spectrum, the Fermi energy can be estimated using the following formula:

$$\varepsilon_F^{(\mathrm{QR})} = k_BT \ln\left[\exp\left(\frac{\pi\hbar^2\langle\Sigma\rangle}{mk_BTa\sqrt{\Sigma_{\mathrm{QR}}}}\right) - 1\right] \simeq \frac{\pi\hbar^2\langle\Sigma\rangle}{m\sqrt{a^2\Sigma_{\mathrm{QR}}}}, \tag{2}$$

where a and $\Sigma_{\mathrm{QR}}^{-1/2}$ are the width of QRs and the lateral distance between QRs (lateral period of the QR array), respectively. In the case of QRIPs with rather narrow QRs having only one energy level of lateral quantization, the electron system in each QR constitutes a one-dimensional gas. In this case, one obtains

$$\varepsilon_F^{(\mathrm{QR})} \simeq \frac{\pi^2\hbar^2\langle\Sigma\rangle^2}{8m\Sigma_{\mathrm{QR}}}. \tag{3}$$

Relatively large QDs (in the lateral directions) can have several quantum shells and be able to accept a rather large number of electrons. In the most experiments, QDIPs with just such QDs were studied. A QD array with QDs of this type can be considered as a disintegrated QW. Since many quantum shells can be occupied by electrons in these QDs, calculating the electron Fermi energy, one can neglect the discreteness of their spectrum. In this case, for the activation energy one can use the formula similar to that for QWs. However, one needs to take into account that real sheet electron density inside the QD equals $\langle\Sigma\rangle/a^2\Sigma_{\mathrm{QD}}$. Here a and Σ_{QD} are the QD lateral size and the sheet density of QDs in each array, respectively. The QD density is limited by the condition of a weak overlap of the wavefunctions of neighbouring QDs [2]. Otherwise, the probability of the electron photoemission by normal incident IR can become fairly small (see, for example, [28]). This means that the product $a^2\Sigma_{\mathrm{QD}}$ should not be too close to unity.

As a result, one obtains

$$\varepsilon_F^{(\mathrm{QD})} \simeq k_BT \ln\left[\exp\left(\frac{\pi\hbar^2\langle\Sigma\rangle}{mk_BTa^2\Sigma_{\mathrm{QD}}}\right) - 1\right] \simeq \frac{\pi\hbar^2\langle\Sigma\rangle}{ma^2\Sigma_{\mathrm{QD}}}. \tag{4}$$

Both simplified and rather detailed device models of QWIPs with tunnelling and thermionic injection [29–32] lead to the following relationship which provides an estimate of the thermal dark current:

$$j_{\mathrm{th}} \simeq \frac{e\mathcal{G}_{\mathrm{th}}}{\langle p\rangle}, \tag{5}$$

where e is the electron charge, $\mathcal{G}_{\mathrm{th}}$ is the rate of thermoemission (per unit area of a QW, a QR or QD array), and $\langle p\rangle$ is the average probability of the capture of a mobile electron passing across a QW.

Considering equations (1), (2), (4) and (5) and introducing $\Sigma_T = mk_BT/\pi\hbar^2$, the density of thermal dark current can be presented as

$$j_{\mathrm{th}}^{(\mathrm{QWIP})} \propto \frac{1}{\langle p\rangle^{(\mathrm{QW})}}\left[\exp\left(\frac{\langle\Sigma\rangle}{\Sigma_T}\right) - 1\right]\exp\left(-\frac{\varepsilon_i}{k_BT}\right) \simeq \frac{1}{\langle p\rangle^{(\mathrm{QW})}}\exp\left(\frac{\langle\Sigma\rangle}{\Sigma_T}\right)\exp\left(-\frac{\varepsilon_i}{k_BT}\right), \tag{6}$$

$$j_{\mathrm{th}}^{(\text{L-QRIP})} \propto \frac{\sqrt{a^2\Sigma_{\mathrm{QR}}}}{\langle p\rangle^{(\mathrm{QR})}}\left[\exp\left(\frac{\langle\Sigma\rangle}{\Sigma_T\sqrt{a^2\Sigma_{\mathrm{QR}}}}\right) - 1\right] \times \exp\left(-\frac{\varepsilon_i}{k_BT}\right) \simeq \frac{\sqrt{a^2\Sigma_{\mathrm{QR}}}}{\langle p\rangle^{(\mathrm{QR})}}\exp\left(\frac{\langle\Sigma\rangle}{\Sigma_T\sqrt{a^2\Sigma_{\mathrm{QR}}}}\right) \times \exp\left(-\frac{\varepsilon_i}{k_BT}\right), \tag{7}$$

$$j_{\mathrm{th}}^{(\text{L-QDIP})} \propto \frac{(a^2\Sigma_{\mathrm{QD}})}{\langle p\rangle^{(\mathrm{QD})}}\left[\exp\left(\frac{\langle\Sigma\rangle}{\Sigma_Ta^2\Sigma_{\mathrm{QD}}}\right) - 1\right]\exp\left(-\frac{\varepsilon_i}{k_BT}\right) \simeq \frac{(a^2\Sigma_{\mathrm{QD}})}{\langle p\rangle^{(\mathrm{QD})}}\exp\left(\frac{\langle\Sigma\rangle}{\Sigma_Ta^2\Sigma_{\mathrm{QD}}}\right)\exp\left(-\frac{\varepsilon_i}{k_BT}\right). \tag{8}$$

If the densities of QR and QD arrays tend to their maxima $\Sigma_{\mathrm{QR}} = a^{-2}$ and $\Sigma_{\mathrm{QD}} = a^{-2}$, the distinctions between QW, on the one hand, and QR and QD arrays, on the other, vanish. In this case, one can set $\langle p\rangle^{(\mathrm{QR})} = \langle p\rangle^{(\mathrm{QD})} = \langle p\rangle^{(\mathrm{QW})}$, and equations (6)–(8), naturally, lead to $j_{\mathrm{th}}^{(\text{L-QRIP})} = j_{\mathrm{th}}^{(\text{L-QDIP})} = j_{\mathrm{th}}^{(\mathrm{QWIP})}$.

Using equations (3) and (5), for rather narrow QRs we arrive at

$$j_{\mathrm{th}}^{(\text{S-QRIP})} \propto \frac{\sqrt{a^2\Sigma_{\mathrm{QR}}}}{\langle p\rangle^{(\mathrm{QR})}}\exp\left(\frac{\pi\langle\Sigma\rangle^2}{8\Sigma_T\Sigma_{\mathrm{QR}}}\right)\exp\left(-\frac{\varepsilon_i}{k_BT}\right). \tag{9}$$

In the case of relatively small QDs having a single quantum shell (with maximum two electrons), considering that $\varepsilon_a = \varepsilon_i$ (see figure 3), for the thermoemission rate one obtains

$$j_{\mathrm{th}}^{(\text{S-QDIP})} \propto \frac{1}{\langle p\rangle^{(\mathrm{QD})}}\frac{\langle\Sigma\rangle}{2\Sigma_{\mathrm{QD}}}\exp\left(-\frac{\varepsilon_i}{k_BT}\right). \tag{10}$$

4. Capture probability

The electron capture probability is determined by many factors: structural and material parameters of QWs and inter-QW barriers [33], energy distribution of mobile electrons [34–36], and so on. The energy distribution of mobile electrons affects the average capture probability because, in part, the dominant capture mechanism is associated with the emission of optical phonons by electrons. Therefore, a mobile electron having the kinetic energy exceeding the optical phonon energy can not directly be captured. Electron heating results in a decrease of the fraction of low-energy electrons and, hence, in a decrease in the average capture probability. Since the energy distribution of mobile electrons is determined by the electric field, which can give rise to a significant electron heating [34–36] with the average kinetic energy of mobile electrons $\langle\varepsilon\rangle \gg k_BT$, the average capture probability exhibits a steep roll-off with increasing electric field. This, according

to equation (10), results in a steeply increasing dark current–voltage characteristic.

The processes of the electron capture in QRIPs and QDIPs, as already pointed out above, have distinctive features. First of all, the quasi-discreteness and discreteness of the electron spectra in QRs in QDs can substantially affect the electron capture. This effect can be, particularly, pronounced in QDIPs when the quantum level separation exceeds the energy of polar optical phonons leading to the phonon 'bottleneck' in the electron capture. Second, due to a limited number of the quantum states in each QD, these states can be fully occupied preventing the electron capture (because of the Pauli principle) under some conditions, for example, excessive doping of the active region and/or large applied voltage. Third, in QRIPs and QDIPs with low-density QR and QD arrays, the negative potential of QRs and QDs charged by the captured electrons can result in an effective repulsion of mobile electrons. This can be a substantial factor limiting their capture [37–42]. In particular, in QDIPs, the capture probability can be presented in the following form [38, 39, 41]:

$$\langle p\rangle^{(\mathrm{QD})} \propto (a^2\Sigma_{\mathrm{QD}})\frac{[\max N\Sigma_{\mathrm{QD}} - \langle\Sigma\rangle]}{\max N\Sigma_{\mathrm{QD}}} \times \exp\left[-\frac{e^2}{\langle\varepsilon\rangle C_{\mathrm{QD}}}\frac{\langle\Sigma\rangle}{\Sigma_{\mathrm{QD}}}\right], \tag{11}$$

where C_{QD} is the efficient QD capacitance which depends on the QD size as well as the spacings between QDs. This formula describes the variation of the capture probability with changing average QD occupancy $N = \langle\Sigma\rangle/\max N\Sigma_{\mathrm{QD}}$, where max N is the maximum number of electrons which can be accepted by a QD. It shows that $\langle p\rangle^{(\mathrm{QD})}$ tends to zero when $\langle\Sigma\rangle$ approaches the maximum value allowed by the Pauli principle, i.e., to max $N\Sigma_{\mathrm{QD}}$. Equation (11) also shows that $\langle p\rangle^{(\mathrm{QD})}$ as a function of $\langle\Sigma\rangle$ contains an exponential factor associated with the effect of the repulsion of mobile electrons. Assuming that $\langle\varepsilon\rangle$ corresponds to the temperature $T = 80$ K and setting $\langle\Sigma\rangle = \Sigma_{\mathrm{QD}}$, $C_{\mathrm{QD}} \simeq 2æa/\pi^{3/2}$ (æ = 12 is the dielectric constant), and $a = 15$ nm, for the exponential factor in equation (11) one obtains $\simeq 0.04$. One can show that the $\langle p\rangle^{(\mathrm{QR})}$ also steeply decreases with increasing $\langle\Sigma\rangle$.

As follows from formulae (6)–(9), the thermal dark current in L-QRIPs and L-QDIPs are fairly sharp functions of $\langle\Sigma\rangle$ and they are steeper than this current in QWIPs. Strongly decreasing $\langle p\rangle^{(\mathrm{QD})} - \langle\Sigma\rangle$ and $\langle p\rangle^{(\mathrm{QR})} - \langle\Sigma\rangle$ dependences result in even more dramatic rise of the thermal dark current in L-QRIPs and L-QDIPs with increasing $\langle\Sigma\rangle$ and its much higher values compared to those in QWIPs.

In contrast to L-QDIP, S-QDIPs with rather dense QD arrays can exhibit lower dark current than QWIPs do. Figures 4 and 5 show the ratio $j_{\mathrm{th}}^{(\mathrm{S\text{-}QDIP})}/j_{\mathrm{th}}^{(\mathrm{QWIP})}$ as a function of the average electron sheet concentration calculated using equations (6) and (10) for different ratios $\langle p\rangle^{(\mathrm{QW})}/\langle p\rangle^{(\mathrm{QD})}$ and different temperatures. The QD density is chosen to be $\Sigma_{\mathrm{QD}} = 5 \times 10^{11}$ cm^{-2} with the maximum possible number of electrons in QDs equal to max $N = 2$. Due to closely packed QDs, we neglected possible weak lateral nonuniformity of the potential of QD arrays. Owing to this, we disregarded the exponential factor in equation (11) and set $\langle p\rangle^{(\mathrm{QW})}/\langle p\rangle^{(\mathrm{QD})} = 2c\Sigma_{\mathrm{QD}}/[2\Sigma_{\mathrm{QD}} - \langle\Sigma\rangle]$. The quantity

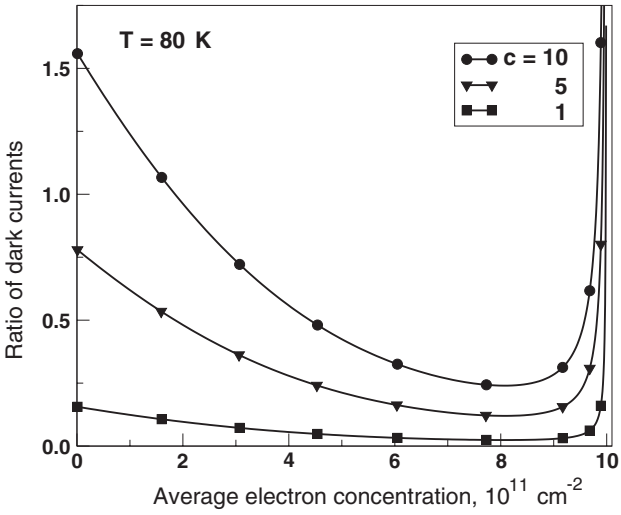

Figure 4. Ratio of dark current in an S-QDIP and in a QWIP as a function of average electron sheet concentration at different ratios of capture probability and $T = 80$ K.

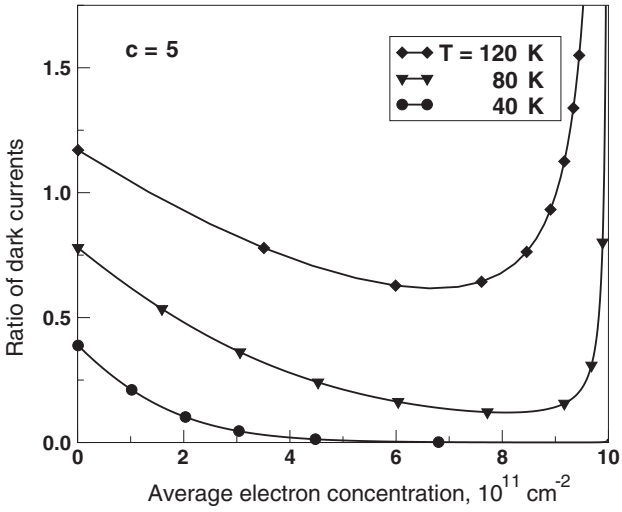

Figure 5. The same as in figure 4 but for different temperatures.

c can vary in a fairly wide range depending on the role of the phonon bottleneck effect in the electron capture. When this effect can be neglected, one has $c \simeq 1$. As follows from figures 4 and 5, even at a large parameter c, the dark current in S-QDIP can be lower that in QWIPs in a certain range of the average electron concentrations. However, the dark current in S-QDIPs becomes rather large when $\langle\Sigma\rangle$ approaches $2\Sigma_{\mathrm{QD}}$ because in this case, due to the Pauli principle, $\langle p\rangle^{(\mathrm{QD})}$ tends to zero.

The wetting layers in the QD arrays can markedly affect the electron capture into QDs. The incorporation of extra barriers between the QD arrays [14] can substantially influence the dynamics and heating of mobile electrons. As a result, the capture processes in QDIPs with such barriers can be different from those in more traditional QDIPs. Both the wetting layers and the extra barriers should result in increasing capture rate, and, therefore, in decreasing dark current. Simultaneously they can result in lowering of the QDIP responsivity (see below).

5. Responsivity and photoelectric gain

Similarly to equation (10), the density of the photocurrent can be expressed via the rate of photoemission from a QW (QR or QD array) by the following equation:

$$j_{\rm ph} \simeq \frac{e\mathcal{G}_{\rm ph}}{\langle p\rangle} = \frac{e\sigma\langle\Sigma\rangle I}{\langle p\rangle}, \tag{12}$$

where $\mathcal{G}_{\rm ph} = \sigma\langle\Sigma\rangle I$ is the rate of photoemission (per unit area), σ is the photoemission cross-section and I is the IR photon flux. According to equation (12), the responsivity of QWIPs, QRIPS and QDIPs can, respectively, be presented as

$$R^{(\rm QWIP)} = \frac{e\sigma^{(\rm QW)}\langle\Sigma\rangle}{\hbar\Omega\langle p\rangle^{(\rm QW)}}, \qquad R^{(\rm QRIP)} = \frac{e\sigma^{(\rm QR)}\langle\Sigma\rangle}{\hbar\Omega\langle p\rangle^{(\rm QR)}}, \qquad R^{(\rm QDIP)} = \frac{e\sigma^{(\rm QD)}\langle\Sigma\rangle}{\hbar\Omega\langle p\rangle^{(\rm QD)}}, \tag{13}$$

where $\hbar\Omega$ is the photon energy. One can see that the rate of photoemission in all the photodetectors under consideration is a rather weak (linear, near linear if the photoemission cross-section depends somehow on the electron concentration) function of the average electron concentration. It is instructive that both the dark current and the responsivity do not explicitly depend on the number of QWs (QR and QD arrays) K in the photodetector.

Under normal operation conditions $\langle p\rangle$ is rather small. This corresponds to the situation when the number of electrons emitted from one QW (one array) is much smaller that the number of the electrons injected by the emitter.

In such a case, the current gain (or photoelectric gain) can be large. This quantity is defined as the ratio of the total flux of the injected electrons $j_{\rm th}/e$ to the total rate of thermoemission from all the QWs $G_{\rm th} = K\mathcal{G}_{\rm th}$ (under dark conditions) or as the ratio of the total flux of the injected electrons $j_{\rm ph}/e$ to the total rate of photoemission from all the QWs $G_{\rm ph} = K\mathcal{G}_{\rm ph}$ (under sufficiently strong illumination), hence, $g = j_{\rm th}/eK\mathcal{G}_{\rm th}$ or $g = j_{\rm ph}/eK\mathcal{G}_{\rm ph}$. Using equation (5) or (12), the current (photoelectric) gain can be estimated as

$$g^{(\rm QWIP)} \simeq \frac{1}{K\langle p\rangle^{(\rm QW)}}, \qquad g^{(\rm QRIP)} \simeq \frac{1}{K\langle p\rangle^{(\rm QR)}}, \qquad g^{(\rm QDIP)} \simeq \frac{1}{K\langle p\rangle^{(\rm QD)}}. \tag{14}$$

Since the electron capture processes in QDIPs can be attenuated due to such reasons as the phonon bottleneck effect, the Pauli principle, and the formation of repulsive potential, the responsivity of QDIPs can be substantially higher than the responsivity of QWIPs. Due to all the above-mentioned reasons or some of them, the QDIP responsivity can be as large as several A/W [23]. Relatively large values of the responsivity are also achieved in QDIPs with lateral structure [20, 21], in which a small capture probability is primarily due to repulsion of mobile electrons by charged QD arrays. However, a small capture probability in QDIPs results in not only high values of the responsivity, but in large dark current as well.

As shown theoretically [30–32], the electron sheet concentration in QWIPs with different mechanisms of the electron injection from the emitter contact into the active region (tunnelling or thermionic) is determined by the donor-sheet concentration (per one QW) in this region Σ_D, the number of QWs K, and the applied voltage V. Generally, the electron sheet concentrations in different QWs in the QWIP can be different. In QWIPs with the tunnelling injection, the electron sheet concentrations in QWs adjacent to the emitter can be either smaller or larger than in the QWIP active region bulk. This is confirmed by numerical modelling of QWIPs [43, 44]. To estimate the average electron sheet concentration $\langle\Sigma\rangle$ one can use the following simple formula:

$$\langle\Sigma\rangle - \Sigma_D \simeq \frac{2C}{e}(V - V_{\rm C}), \tag{15}$$

where C is a coefficient dependent on the number of QWs K, and $V_{\rm C}$ is some characteristic voltage. The latter is determined mainly by the electron injection conditions. In particular, in QWIPs with the tunnelling injection [30, 31] $V_{\rm C} > 0$. However, if the electron injection from the contact into the QWIP active region is of thermionic origin [32], $V_{\rm C} < 0$. Equation (15) explicitly indicates that the total charge of the QWIP active region changes with varying applied voltage. This is because the electric field induces extra electrons in QWs [45, 46]. Similar calculations [37, 38] show that equation (15) can also be used for QDIPs. Equation (15) is in a qualitative agreement with experimental results [47] and computer modelling based on ensemble Monte Carlo particle method [48].

Due to equations (6)–(9), the rate of thermoemission from QWs, QRs and QDs exponentially increases with $\langle\Sigma\rangle$, which, according to equation (15), is a function of the applied voltage. As a result, the dark current–voltage characteristics of QWIPs, QRIPs and QDIPs are very steep in agreement with more detailed calculations and experimental data. Since the photoemission rate is much smoother function of $\langle\Sigma\rangle$ and, therefore, V, the responsivity increases with the bias voltage slower that the dark current.

6. Detectivity

The detector detectivity D^* for a thermally-limited detection can be expressed in terms of the total thermoemission and photoexcitation rates $G_{\rm th} = K\mathcal{G}_{\rm th}$ and $G_{\rm ph} = K\mathcal{G}_{\rm ph}$ from the detector unit area the following form [49]:

$$D^* = \frac{G_{\rm ph}}{2\hbar\Omega I\sqrt{G_{\rm th}}}. \tag{16}$$

The QWIP detectivity can be expressed via the average electron concentration $\langle\Sigma\rangle$ as

$$D^{*(\rm QWIP)} \propto \frac{\sqrt{K}\sigma_{\rm QR}\langle\Sigma\rangle}{\sqrt{\exp\left(\frac{\langle\Sigma\rangle}{\Sigma_T}\right) - 1}}\exp\left(\frac{\varepsilon_i}{k_BT}\right) \simeq \sqrt{K}\sigma_{\rm QR}\langle\Sigma\rangle\exp\left(-\frac{\langle\Sigma\rangle}{2\Sigma_T}\right)\exp\left(\frac{\varepsilon_i}{2k_BT}\right). \tag{17}$$

The detectivities of L-QRIPs and S-QRIPs are given by the following equations, respectively:

$$D^{*(\rm L\text{-}QRIP)} \propto \frac{\sqrt{K}\sigma_{\rm QR}\langle\Sigma\rangle}{(a^2\Sigma_{\rm QR})^{1/4}}\frac{\exp\left(\frac{\varepsilon_i}{k_BT}\right)}{\sqrt{\exp\left(\frac{\langle\Sigma\rangle}{\Sigma_T\sqrt{a^2\Sigma_{\rm QR}}}\right) - 1}} \simeq \frac{\sqrt{K}\sigma_{\rm QW}\langle\Sigma\rangle}{(a^2\Sigma_{\rm QR})^{1/4}}\exp\left(-\frac{\langle\Sigma\rangle}{2\Sigma_T\sqrt{a^2\Sigma_{\rm QR}}}\right)\exp\left(\frac{\varepsilon_i}{2k_BT}\right), \tag{18}$$

$$D^{*(\text{S-QRIP})} \propto \frac{\sqrt{K}\sigma_{\text{QR}}}{(a^2\Sigma_{\text{QR}})^{1/4}}\langle\Sigma\rangle \exp\left(-\frac{\pi^2\langle\Sigma\rangle^2}{16\Sigma_T\Sigma_{\text{QR}}}\right) \times \exp\left(\frac{\varepsilon_i}{2k_BT}\right). \tag{19}$$

For the detectivities of L-QDIPs and S-QDIPs one obtains, respectively,

$$D^{*(\text{L-QDIP})} \propto \frac{\sqrt{K}\sigma_{\text{QD}}\langle\Sigma\rangle}{\sqrt{a^2\Sigma_{\text{QR}}}} \frac{\exp\left(\frac{\varepsilon_i}{k_BT}\right)}{\sqrt{\exp\left(\frac{\langle\Sigma\rangle}{\Sigma_T a^2\Sigma_{\text{QD}}}\right)-1}} \simeq \frac{\sqrt{K}\sigma_{\text{QD}}\langle\Sigma\rangle}{\sqrt{a^2\Sigma_{\text{QD}}}} \exp\left(-\frac{\langle\Sigma\rangle}{2\Sigma_T a^2\Sigma_{\text{QD}}}\right)\exp\left(\frac{\varepsilon_i}{2k_BT}\right), \tag{20}$$

$$D^{*(\text{S-QDIP})} \propto \sqrt{K}\sigma_{\text{QD}}\sqrt{2\Sigma_{\text{QD}}\langle\Sigma\rangle}\exp\left(\frac{\varepsilon_i}{2k_BT}\right). \tag{21}$$

Relationships (17)–(21) show that the detectivity of detectors under consideration is proportional to $\sqrt{K}$, i.e., the detectors with large number of QWs (QR or QD arrays) exhibit higher detectivity (see, for example, [50]). Using equations (17)–(20), one can obtain formulae for the maximum values of the detectivity at a given temperature which are reached at certain values of $\langle\Sigma\rangle$, i.e., at certain doping levels and applied voltages (generally different for different types of the photodetectors):

$$\max D^{*(\text{QWIP})} \propto 2\sqrt{K}\sigma_{\text{QW}}\Sigma_T\exp\left(\frac{\varepsilon_i}{2k_BT}-1\right), \tag{22}$$

$$\max D^{*(\text{L-QRIP})} \propto 2\sqrt{K}\sigma_{\text{QR}}(a^2\Sigma_{\text{QR}})^{1/4}\Sigma_T\exp\left(\frac{\varepsilon_i}{2k_BT}-1\right), \tag{23}$$

$$\max D^{*(\text{S-QRIP})} \propto \sqrt{K}\sigma_{\text{QR}}\frac{\sqrt{8\Sigma_T\Sigma_{\text{QR}}}}{\pi(a^2\Sigma_{\text{QR}})^{1/4}}\exp\left(\frac{\varepsilon_i}{2k_BT}-\frac{1}{2}\right), \tag{24}$$

$$\max D^{*(\text{L-QDIP})} \propto 2\sqrt{K}\sigma_{\text{QD}}\Sigma_T\sqrt{a^2\Sigma_{\text{QD}}}\exp\left(\frac{\varepsilon_i}{2k_BT}-1\right). \tag{25}$$

As follows from relationship (21), the detectivity of S-QDIPs monotonically increases with increasing $\langle\Sigma\rangle$. However, the latter quantity is limited due to the Pauli principle by the value $2\Sigma_{\text{QD}}$. As mentioned above (see also [2]), the current gain can dramatically increase when $\langle\Sigma\rangle$ tends to $2\Sigma_{\text{QD}}$ leading to very large dark current and responsivity simultaneously. Nevertheless, to estimate $\max D^{*(\text{S-QDIP})}$ in such QDIPs, we set $\langle\Sigma\rangle = 2\Sigma_{\text{QD}}$ in relationship (21). As a result, we obtain

$$\max D^{*(\text{S-QDIP})} \propto 2\sqrt{K}\sigma_{\text{QD}}\Sigma_{\text{QD}}\exp\left(\frac{\varepsilon_i}{2k_BT}\right). \tag{26}$$

Relationships (22), (23) and (25) yield the following formulae for the ratios of the detectivities:

$$\frac{\max D^{*(\text{L-QRIP})}}{\max D^{*(\text{QWIP})}} \simeq \frac{\sigma_{\text{QR}}}{\sigma_{\text{QW}}}(a^2\Sigma_{\text{QR}})^{1/4}, \tag{27}$$

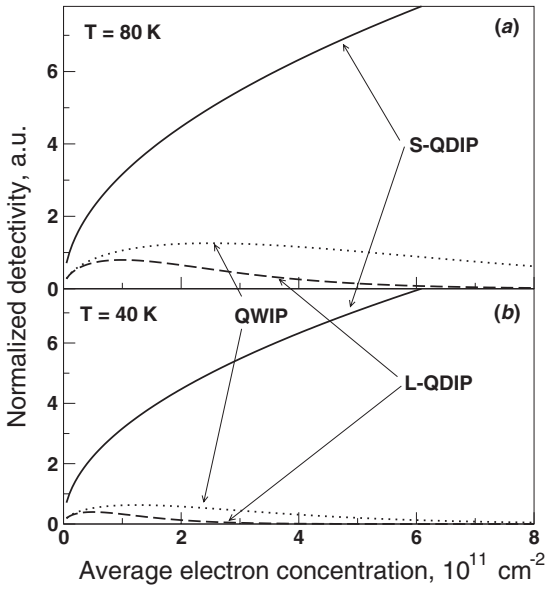

Figure 6. Normalized detectivities of QWIP, L-QDIP and S-QDIP versus average electron sheet concentration at (*a*) $T = 80$ K and (*b*) $T = 40$ K.

$$\frac{\max D^{*(\text{L-QDIP})}}{\max D^{*(\text{QWIP})}} \simeq \frac{\sigma_{\text{QD}}}{\sigma_{\text{QW}}}\sqrt{a^2\Sigma_{\text{QD}}}. \tag{28}$$

Simultaneously, relationships (24) and (26) lead to

$$\frac{\max D^{*(\text{S-QRIP})}}{\max D^{*(\text{QWIP})}} \simeq 0.8\frac{\sigma_{\text{QR}}}{\sigma_{\text{QW}}}(a^2\Sigma_{\text{QR}})^{-1/4}\sqrt{\frac{\Sigma_{\text{QR}}}{\Sigma_T}} \tag{29}$$

and

$$\frac{\max D^{*(\text{S-QDIP})}}{\max D^{*(\text{QWIP})}} \simeq 2.7\frac{\sigma_{\text{QD}}}{\sigma_{\text{QW}}}\frac{\Sigma_{\text{QD}}}{\Sigma_T}. \tag{30}$$

The dependences of the QWIP, L-QDIP and S-QDIP detectivities (normalized by factor $\exp(\varepsilon_i/2k_BT)$) on the average electron sheet concentration per one QW and one QD array calculated using formulae (17), (20) and (21) are plotted in figure 6. We set for simplicity $\sigma_{\text{QW}} = \sigma_{\text{QD}}$. It is assumed that $\Sigma_{\text{QD}} = 1\times10^{11}$ cm^{-2} in an L-QDIP ($a^2\Sigma_{\text{QD}} = 0.4$) and $\Sigma_{\text{QD}} = 5\times10^{11}$ cm^{-2} (so the product $a^2\Sigma_{\text{QD}}$ is approximately the same for both QDIPs). Figure 6 shows that even at the QD density markedly smaller than the maximum possible density (see below), the detectivity of S-QDIPs can significantly exceed that of QWIPs. The superiority of S-QDIPs over QWIPs in detectivity can particularly be pronounced at low temperatures.

Let us estimate $\max\Sigma_{\text{QD}}/\Sigma_T$ which determines the ratio of the S-QDIP and QWIP responsivities. The QD density in QDIPs is limited by the requirement of a weak overlap of the wavefunctions of neighbouring QDs [2]. Due to such an overlap, a narrow miniband can arise. Its width in QDIPs is estimated as

$$\Delta \simeq \varepsilon_i\exp\left(-\frac{1}{\hbar^2}\sqrt{\frac{2m\varepsilon_i}{\Sigma_{\text{QD}}}}\right). \tag{31}$$

Broadening of the ground states in QDs into the miniband does not affect the activation energy if $\Delta \ll 2k_BT$. Taking

into account this inequality and using equation (31), we obtain the following condition:

$$\Sigma_{\rm QD} < \frac{2m\varepsilon_i}{\hbar^2 \ln^2(\varepsilon_i/2k_BT)}. \quad (32)$$

Condition (32) can be rewritten as

$$\frac{\Sigma_{\rm QD}}{\Sigma_T} < 2\pi \left(\frac{\varepsilon_i}{k_BT}\right) \frac{1}{\ln^2(\varepsilon_i/2k_BT)}. \quad (33)$$

Using equation (30) and condition (33), one can obtain the following inequality:

$$\frac{\max D^{*(\text{S-QDIP})}}{\max D^{*(\text{QWIP})}} < 17 \left(\frac{\sigma_{\rm QD}}{\sigma_{\rm QW}}\right) \left(\frac{\varepsilon_i}{k_BT}\right) \frac{1}{\ln^2(\varepsilon_i/2k_BT)} = \left(\frac{\sigma_{\rm QD}}{\sigma_{\rm QW}}\right) \Gamma, \quad (34)$$

in which the right-hand side can be fairly large at not too small ratio $\sigma_{\rm QD}/\sigma_{\rm QW}$ because of $\Gamma \gg 1$. Indeed, choosing $\varepsilon_i = 100$ meV and $T = 40$–80 K, one can obtain $\Gamma \simeq 390$–425.

Taking into account relationship (34), one may conclude that S-QDIPs with the QD densities close to the maximum value can really exhibit much larger detectivity than QWIPs if the photoemission cross-section $\sigma_{\rm QD}$ for normal IR incidence and $\sigma_{\rm QW}$ for inclined incidence are close to each other or, at least, the former is not very small. However, one needs to note that the ratio of the photoionization cross-sections can pronouncedly depend on the structure of QR and QD arrays [51, 52].

7. Conclusions

We compared QWIPs, QRIPs and QDIPs . This resulted in the following conclusions:

- QRIPs and QDIPs can exhibit much higher responsivity than QWIPs due to lower capture probability and, therefore, larger photoelectric gain. Higher responsivity is inevitably accompanied by higher dark current, because it is amplified with the same gain.
- QRIPs and QDIPs based on low-density arrays of relatively large QRs and QDs (L-QRIPs and L-QDIPs, in our terms) should definitely be inferior to QWIPs in detectivity.
- QRIPs and, particularly, QDIPs based on extremely dense arrays of narrow QRs and small QDs, in which the bound electrons are really one-dimensional and zero-dimensional, respectively, can significantly surpass QWIPs in detectivity.

Acknowledgments

The authors are thankful to Mr A Satou for assistance.

References

[1] Ryzhii V (ed) 2003 *Intersubband Infrared Photodetectors* (Singapore: World Scientific)
[2] Ryzhii V 1996 *Semicond. Sci. Technol.* **11** 759
[3] Ryzhii V, Khmyrova I, Ryzhii M and Ershov M 1996 *J. Physique* IV **6** C3–157
[4] Berryman K W, Lyon S A and Segev M 1997 *Appl. Phys. Lett.* **70** 1861
[5] Phillips J, Kamath K and Bhattacharya B 1998 *Appl. Phys. Lett.* **72** 2020
[6] Kim S, Mohseni H, Erdtmann M, Michel E, Jelen C and Razeghi M 1998 *Appl. Phys. Lett.* **73** 963
[7] Pan D, Towe E and Kennerly S 1998 *Appl. Phys. Lett.* **73** 1937
[8] Maimon S, Finkman E, Bahir G, Schacham S E, Garcia J M and Petroff P M 1998 *Appl. Phys. Lett.* **73** 2003
[9] Xu S J, Chua S J, Mei T, Wang X C, Zhang X H, Karunasiri G, Fan W J, Wang C H, Jiang J, Wang S and Xie X G 1998 *Appl. Phys. Lett.* **73** 3153
[10] Horiguchi N, Futatsugi T, Nakata Y, Yokoyama N, Mankad T and Petroff P M 1999 *Japan. J. Appl. Phys.* **38** 2559
[11] Phillips J, Bhattacharya P, Kennerly S W, Beekman D W and Dutta M 1999 *IEEE J. Quantum Electron.* **35** 936
[12] Pan D, Towe E and Kennerly S 1999 *Appl. Phys. Lett.* **75** 2719
[13] Ye Z, Campbell J C, Chen Z, Kim E-T and Madhukar A 2002 *IEEE J. Quantum Electron.* **38** 1234
[14] Tang S-F, Lin S-Y and Lee S-C 2002 *IEEE Trans. Electron Devices* **49** 1341
[15] Yakimov A I, Dvurechenskii A V, Proskuryakov Y Yu, Nikiforov A I, Pchelyakov O P, Teys S A and Gutakovskii A K 1999 *Appl. Phys. Lett.* **75** 1413
[16] Rappaport N, Finkman E, Brunhes T, Boucaud P, Sauvage S, Yam N, Thanh V Le and Boucier D 2000 *Appl. Phys. Lett.* **77** 3224
[17] Liu H C, Gao M, McCaffrey J, Wasilewski Z R and Fafard S 2001 *J. Appl. Phys.* **78** 79
[18] Yakimov A I, Dvurechenskii A V, Nikiforov A I and Proskuryakov Y Y 2001 *J. Appl. Phys.* **89** 5676
[19] Boucaud P, Brunhes T, Sauvage S, Yam N, Thanh V Le, Boucier D and and Rappaport N 2001 Quantum dots *Phys. Status Solidi* a **224** 233
[20] Miesner C, Brunner K and Abstreiter G 2001 *Phys. Status Solidi* a **224** 605
[21] Lee S-W, Hirakawa K and Shimada Y 1999 *Appl. Phys. Lett.* **75** 1428
[22] Rokhinson L P, Chen C J, Tsui D C, Vawter G A and Choi K K 1999 *Appl. Phys. Lett.* **74** 759
[23] Raghavan S, Rotella P, Stinz A, Fuchs B, Krishna S, Morath C, Cardimona D A and Kennerly S W 2002 *Appl. Phys. Lett.* **81** 1369
[24] Towe E and Pan D 2000 *IEEE J. Sel. Top. Quantum Electron.* **6** 408
[25] Ryzhii V, Khmyrova I, Ryzhii M, Pipa V, Mitin V and Willander M 2001 *Proc. SPIE* **4288** 396
[26] Bhattacharya P, Stiff-Roberts A D, Krishna S and Kennerly S 2002 *Proc. Soc. Photo-Opt. Instrum. Eng.* **4646** 100
[27] Ryzhii V and Khmyrova I 2003 *Proc. Soc. Photo-Opt. Instrum. Eng.* **4986** 190
[28] Helm M, Hilber W, Fromherz T, Peters F M, Alavi K and Psthar R N 1994 *Quantum Well Intersubband Transition Physics and Devices* ed H C Liu, B F Levine and J Y Andersson (Dordrecht: Kluwer) p 291
[29] Liu H C 1992 *Appl. Phys. Lett.* **60** 1507
[30] Ryzhii V 1997 *J. Appl. Phys.* **81** 6442
[31] Ryzhii V and Liu H C 1999 *Japan. J. Appl. Phys.* **38** 5815
[32] Ryzhii V, Ryzhii M and Liu H C 2002 *J. Appl. Phys.* **92** 207
[33] Rosencher E, Vinter B, Luc F, Thibaudeau L, Bois P and Nagle J 1994 *IEEE Trans. Quantum Electron.* **30** 2875
[34] Ryzhii M and Ryzhii V 1999 *Japan. J. Appl. Phys.* **38** 5922
[35] Ryzhii M, Ryzhii V and Willander M 1999 *Japan. J. Appl. Phys.* **38** 6650
[36] Kochman B, Stiff-Roberts D, Chakrabarti S, Phillips J D, Krishna S and Bhattacharya P 2003 *IEEE J. Quantum Electron.* **39** 459
[37] Ryzhii V, Pipa V, Khmyrova I, Mitin V and Willander M 2000 *Japan. J. Appl. Phys.* **39** L1283
[38] Ryzhii V, Khmyrova I, Pipa V, Mitin V and Willander M 2001 *Semicond. Sci. Technol.* **16** 331

[39] Ryzhii V 2001 *Japan. J. Appl. Phys.* **40** L148
[40] Ryzhii V, Khmyrova I, Mitin V, Stroscio M and Willander M 2001 *Appl. Phys. Lett.* **78** 3523
[41] Ryzhii V 2001 *Appl. Phys. Lett.* **78** 3346
[42] Sergeev A, Mitin V and Stroscio M 2002 *Physica* B **316–317** 369
[43] Ershov M, Ryzhii V and C Hamaguchi 1995 *Appl. Phys. Lett.* **67** 3147
[44] Sa'ar A, Mermelstein C, Schneider H, Schoenbein C and Walther M 1998 *IEEE Photonics Technol. Lett.* **10** 1470
[45] Luryi S 1985 *IEEE Electron Device Lett.* **6** 78
[46] Ryzhii V and Ershov M 1995 *Semicond. Sci. Technol.* **10** 687
[47] Duboz J-Y, Liu H C, Wasilewski Z R, Byloss M and Dudek R 2003 *J. Appl. Phys.* **93** 1320
[48] Ryzhii M, Ryzhii V and Mitin V 2002 *4th Int. Conf. Low Dimensional Structures and Devices (Fortaleza, Brazil)* abstracts p WeO-2
[49] Grave I and Yariv A 1992 *Intersubband Transitions in Quantum Wells* ed E Rosencher, B Vinter and B Levine (New York: Plenum) p 15
[50] Choi K K 1997 *The Physics of Quantum Well Infrared Photodetectors* (Singapore: World Scientific)
[51] Vasanelli A, De Giorgi M, Ferreira R, Cingolani R and Bastard G 2001 *Physica* E **11** 41
[52] Li L-X, Sun S and Chang Y-C 2003 *Infrared Phys. Technol.* **44** 57